

AD-A262 805

2



PL-TR-92-2286

**KINETIC STUDIES OF IONOSPHERIC TRANSPORT
IN THE POLAR CAP AND AURORAL ZONE**

Dwight T. Decker

**INSTITUTE FOR SPACE RESEARCH
Boston College
Chestnut Hill, Massachusetts 02167**

3 November 1992

**FINAL REPORT
(6 July 1988 - 30 December 1992)**

Approved for public release; distribution unlimited

DTIC
SELECTED
MAR 13 1993
S E D



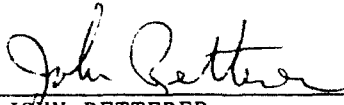
**PHILLIPS LABORATORY
Directorate of Geophysics
AIR FORCE MATERIEL COMMAND
HANSCOM AIR FORCE BASE, MA 01731-5000**

98 098

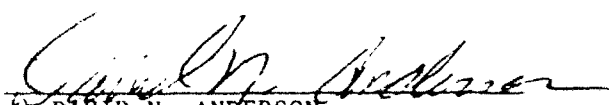
93-05477



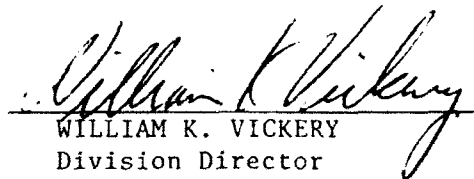
"This technical report has been reviewed and is approved for publication"



JOHN RETTERER
Contract Manager



DAVID N. ANDERSON
Branch Chief



WILLIAM K. VICKERY
Division Director

This report has been reviewed by the ESC Public Affairs Office (PA) and is releasable to the National Technical Information Service (MTIS)

Qualified requestors may obtain additional copies from the Defense Technical Information Center. All others should apply to the National Technical Information Service.

If your address has changed, or if you wish to be removed from the mailing list, or if the addressee is no longer employed by your organization, please notify PL/TSI, Hanscom AFB, MA 01731-5000. This will assist us in maintaining a current mailing list.

Do not return copies of this report unless contractual obligations or notices on a specific document requires that it be returned.

REPORT DOCUMENTATION PAGE

Public reporting burden for this collection of information is estimated to average 1 hour per response, including the time for reviewing instructions, searching existing data sources, gathering and maintaining the data needed, and completing and reviewing the collection of information. Send comments regarding this burden estimate or any aspect of this collection of information, including suggestions for reducing this burden, to Washington Headquarters Services, Directorate for Information Operations and Reports, Room 1224, 1601 G Street, NW, Washington, DC 20540-6001, and to the Office of Management and Budget, Paperwork Reduction Project (0707-0188), Washington, DC 20503.

1. AGENCY USE ONLY (leave blank)		2. REPORT DATE 11/3/97	3. REPORT TYPE AND DATES COVERED FINAL 7/6/88 12/30/97	
4. TITLE AND SUBTITLE Kinetic Studies of Ionospheric Transport in the Polar Cap and Auroral Zone			5. FUNDING NUMBERS FIM 8-88-1-0000 PE 021011 PR 4043 TA 07 WB AD	
6. AUTHOR(S) Dwight T. Decker				
7. PERFORMING ORGANIZATION NAME(S) AND ADDRESS(ES) Boston College Institute for Space Research Chestnut Hill MA 02167			8. PERFORMING ORGANIZATION REPORT NUMBER BC-ISR-97-01	
9. SPONSORING/MONITORING AGENCY NAME(S) AND ADDRESS(ES) Phillips Laboratory Hanscom Air Force Base MA 01731-5000 Contract Manager: John Retterer/GPIM			10. SPONSORING/MONITORING AGENCY REPORT NUMBER PL-TR-92-2256	
11. SUPPLEMENTARY NOTES				
12a. DISTRIBUTION / AVAILABILITY STATEMENT Approved for public release; distribution unlimited			12b. DISTRIBUTION CODE	
13. ABSTRACT (Maximum 200 words) We have studied and modeled several of the important coupling processes that involve particle and energy flow into and within the ionosphere in the polar cap and auroral zone. Understanding these coupling processes helps us better understand the response of the polar ionosphere to external stimuli, and thus helps us understand its structure and day-to-day variability. Modern models of the inner magnetosphere require an accurate treatment of ionospheric precipitation and backscatter to properly describe the population of the plasma sheet. We have developed a detailed kinetic model of the electron population in the inner portion of the magnetosphere, including the effects of convection, pitch angle scattering, precipitation, and backscatter. (Continued on reverse)				
14. SUBJECT TERMS Diffuse aurora; Kinetic theory; Proton precipitation; Photoelectrons; Plasma simulation; Monte Carlo simulation; Ionospheric patches			15. NUMBER OF PAGES 34	
			16. PRICE CODE	
17. SECURITY CLASSIFICATION OF REPORT UNCLASSIFIED	18. SECURITY CLASSIFICATION OF THIS PAGE UNCLASSIFIED	19. SECURITY CLASSIFICATION OF ABSTRACT UNCLASSIFIED	20. LIMITATION OF ABSTRACT SAR	

Using numerical solutions of an electron transport equation with appropriate boundary conditions and sunlit polar cap observations, we find that two energetic electron populations (photoelectron and polar rain) are present and are needed to explain polar cap observations.

Recently, the first self-consistent theory for the combined electron-proton-hydrogen atom aurora has been developed. We present the first test of this fully coupled three species transport model.

Two dimensional plasma simulations and Monte Carlo simulations have been used to calculate the heating of the ions and electrons as well as the temporal evolution of plasma waves in the supauroral region.

E and F region fluid models have been developed and tested against various observations. We find that our models reproduce much of the observed climatology.

Accession For	
NTIS	<input checked="" type="checkbox"/> CRA&I
DTIC	<input checked="" type="checkbox"/> TAB
Unannounced	<input type="checkbox"/>
Justification	
By	
Distribution /	
Availability Codes	
Dist	Avail and/or Special
A-1	

TABLE OF CONTENTS

ACKNOWLEDGEMENTS	v
1. INTRODUCTION	1
2. IONOSPHERIC ELECTRON FLUXES IN THE DIFFUSE AURORA	1
2.1 One Dimensional Kinetic Model	2
2.2 Two Dimensional Kinetic Model	2
2.3 Future Directions	3
3. ENERGETIC PHOTOELECTRONS AND POLAR CAP PRECIPITATION	3
3.1 Midlatitude Calculation	4
3.2 Polar Cap Calculation	4
3.3 Future Directions	7
4. PROTON-HYDROGEN ATOM PRECIPITATION	7
4.1 Comparisons With Observations	7
4.2 Future Directions	10
5. IONOSPHERIC PLASMA TURBULENCE AND PARTICLE ACCELERATION ASSOCIATED WITH DISCRETE-ARC PRECIPITATION	10
5.1 Two Dimensional Plasma Simulations	11
5.2 Comparisons to Observations	12
5.3 Future Directions	12
6. MODELING THE IONOSPHERIC E-REGION	13
6.1 Auger Electron Effects	13
6.2 Global Modeling	13
6.3 Future Directions	14

TABLE OF CONTENTS
(Continued)

7.	MODELING THE MIDLATITUDE F-REGION	14
7.1	Model Modifications	14
7.2	Theoretical Studies	15
7.3	Comparisons with Observations	18
7.4	Future Directions	21
8.	MODELING THE HIGH-LATITUDE F-REGION	21
8.1	Model Modifications	22
8.2	Theoretical Studies	22
8.3	Future Directions	23
9.	SUMMARY	23
	REFERENCES	26

ACKNOWLEDGEMENTS

The author wishes to thank Mr. Leo F. Power, Jr., the Director of the Institute for Space Research, for his able administrative assistance throughout the duration of this contract.

To the Contract Monitors, Dr. James Whalen and Dr. Antonio Quesada, thanks are extended for their collaboration and assistance.

I wish to thank Barbara Bruno for her excellent job in preparing this document as well as the many previous quarterly reports.

Finally, special thanks to Dr. John Retterer, the original Principal Investigator of this contract, who is responsible for much of the work accomplished in this contract.

1. INTRODUCTION

Many of the properties of the ionospheric polar cap and auroral zone are strongly affected by particle and energy flow between the ionosphere and the magnetosphere. In order to study such coupling processes, we have applied both kinetic descriptions of particle transport and acceleration and fluid descriptions of ambient ionospheric ion densities. To understand and model the physics of kinetic phenomena, we have used plasma and Monte Carlo simulations as well as numerical transport calculations. Our approach has been to develop these models, test them against observations and then refine them accordingly. But often, the available observations are not of the quantities calculated in kinetic models. Rather, it is the effects of kinetic phenomena that are often measured. Thus, in order to test and refine the kinetic models, complementary models are needed that will calculate how the kinetic phenomena affect such quantities as ion densities, ion and electron temperatures, and optical emissions.

In sections two and three, we describe our kinetic modeling of the flow of electrons between the ionosphere and magnetosphere. The next two sections focus on coupling through ion transport and acceleration. Our fluid modeling of the E and F regions are treated in sections six through eight. A final section summarizes the overall accomplishments of this contract.

2. IONOSPHERIC ELECTRON FLUXES IN THE DIFFUSE AURORA

The nighttime high latitude ionosphere (auroral ionosphere) is produced by precipitating particles (electrons and ions) with kinetic energies ranging from .1 to more than 10 keV. The diffuse aurora is a rather uniform, relatively low intensity, oval-shaped band of auroral emissions present at essentially all local times, displaced equatorward of, but usually overlapping, the oval of discrete auroral arcs. The diffuse aurora is generated by kilovolt electrons and protons precipitating from the plasma sheet and interacting with the neutral atmosphere. It was recognized in the late 1960s (Kennel, 1969) that the spatial structure of the diffuse aurora could be explained as a consequence of the coupling of plasma sheet convection towards the Earth and the loss of trapped particle flux by precipitation into the ionosphere. As the flow nears the Earth, convection slows while the widening loss cone and falling bounce time make precipitation more effective. To analyze this situation, Kennel introduced a powerful approximation to describe the effect of pitch angle scattering, namely, the approximation of strong diffusion, that states that an isotropic pitch angle distribution is maintained in the face of all the processes that tend to produce anisotropy. This approximation has wide, but not complete, observational justification, and is of such power in simplifying the calculations of precipitation, that it has been almost universally adopted in calculations of this kind (Fontaine and Blanc, 1983; Wolf, 1983). Examination of the observations in more detail, however, shows that electron flux in the diffuse aurora is not always isotropic over the loss cone (Sharber, 1981) and that the conditions of strong pitch-angle scattering do not apply.

We have developed a model for the structure of the diffuse aurora and the precipitation therein using a full kinetic description of the particle fluxes, so that the inaccurate assumption of isotropy can be abandoned. By including the effects of convection, precipitation, and backscatter along with pitch angle scattering, the structure of the auroral ionosphere can be calculated more completely and with a greater degree of realism than before.

2.1 One Dimensional Kinetic Model

The fundamental equation defining the problem is the bounce-averaged pitch-angle diffusion equation with an advective term describing the effects of plasma-sheet convection. It was realized that eigenfunction treatments of the equation would not be adequate, and that an initial-value solution was necessary, starting with a plasma velocity distribution at a high L-shell and letting the plasma convect Earthward. We have developed the algorithm for this solution. To combine the effects of convection and diffusion on the velocity distribution function over a time step, an "operator-splitting" technique was used in which separate, stable algorithms for advancing the velocity distribution function by convection alone and by diffusion alone are alternately applied to describe their combined effects. The convective algorithm is an integration-along-characteristic-trajectory solution of the Liouville equation, assuming that an electron's magnetic moment and longitudinal invariant are conserved during the time step. The guiding center drift is assumed to be $E \times B$ drift. Hence, the model will simulate the latitudinal dependence of the electron flux. The method was demonstrated to conserve flux-tube particle content over finite time steps, so long as the energy and pitch-angle grids were carefully chosen; in particular, the energy grid must extend to high enough energies to allow for the acceleration due to "adiabatic" compression. To solve the diffusion equation, a finite-difference approximation to the pitch-angle diffusion term was worked out, with special care taken to make the algorithm time-centered to help insure stability. The result is of the Crank-Nicholson form. The boundary condition on the pitch-angle derivative of the velocity distribution at small pitch angle is important because it determines the flux out of the trapped distribution that is the net precipitative flux into the ionosphere. This flux is determined by the boundary-layer treatment of the loss cone in velocity space, coupled with a transport treatment of atmospheric backscatter and secondary production. To achieve time-centering, this flux is calculated at the half time steps. All finite-difference expressions are carried out consistently to second order in pitch angle spacing; this promotes the cancellation of truncation error in evaluating integral fluxes.

When pitch angle scattering is not strong, the results of the model show that precipitation does not empty a convecting flux tube before it has drifted past the equatorward edge of the diffuse aurora. Thus, some other mechanism must be introduced to explain the observed drop-off of precipitation at the edge. Others have determined that the Earthward boundary of the convective motion of particles injected from the tail can explain the energy dependence of the boundary in a number of events. We have incorporated drift-boundary limitation of flux into the kinetic model. One benefit of having the equatorward edge of the diffuse aurora limited only by drift boundaries is that in individual events, observation of the boundary then gives us a direct handle on the magnitude of the convection electric field; when the boundary is determined by exhaustion of the flux tube, the position of the boundary depends on the combination of the effects of the strength of pitch angle scattering and the drift velocity, and no direct means of determining the convection field through the precipitation pattern exists.

2.2 Two Dimensional Kinetic Model

The two dimensional version of our model requires that the guiding center drift be a combination of $E \times B$ and gradient/curvature drifts. This allows the model to map out the entire two dimensional structure of the band of diffuse aurora precipitation. At present, the model is too computationally expensive to be applied to the large number of trajectories needed to resolve the details of both the invariant-latitude and local-time variations of the flux, and only the coarsest local-time variations have been admitted into the model. This

has been justified by the observed smooth local-time structure of the diffuse-auroral precipitation.

Nevertheless, statistical studies of the precipitation do find significant local-time structure which it would be interesting and important to model in full detail. As a first step toward such a model, we have developed a test-bed two dimensional plasma-sheet convection model with which to explore the consequences of the two dimensional nature of plasma sheet convection. This model uses the popular assumption of isotropic pitch-angle distributions, but is structured in a way similar to our full kinetic model so that as more efficient algorithms for the pitch-angle scattering and atmospheric transport are developed, they can be incorporated into the two-d model for realism. As a first application of the two-d model, a loss-less flow was studied, demonstrating how the limits on inward convection on the nightside, caused by the energy-dependent gradient/curvature drifts of the electrons, can produce a realistic looking equatorward edge for the diffuse aurora.

2.3 Future Directions

With a kinetic model for the electron flux in the diffuse aurora developed, several applications of the model can be considered. Possible future investigations include the following: considerable insight into the form of the electron flux can be obtained by studying the ways in which it varies when the functional inputs to the model, such as the initial flux, the diffusion coefficient, and the electric potential, are varied. Such a systematic study of these variations is obviously required. Despite the complexity of the phenomena that control the electron flux, the resulting form is of remarkable simplicity. From the complicated output of the model, we would like to be able to extract a simple analytical explanation of the electron-flux form. Such results could be incorporated into global models of the inner magnetosphere. Finally, because one portion of the model describes the atmospheric transport of the precipitating electrons, it is to be noted that among the results of the model is the energy deposited in the ionosphere by the precipitating electrons. This quantity can be used to estimate ionospheric conductivities, optical emissions, and the electron density profile in the E region of the ionosphere.

3. ENERGETIC PHOTOELECTRONS AND POLAR CAP PRECIPITATION

The Low Altitude Plasma Instrument (LAPI) onboard the Dynamics Explorer 2 satellite has observed an energetic electron population (with energies between 60 and 850 eV) in the daytime topside ionosphere. This energetic population exists, together with the "classical" photoelectrons (at energies less than 60 eV) observed by earlier satellites and rocket experiments. Preliminary analysis of this data suggests that this energetic population is produced by soft solar X-ray fluxes in the same way that EUV (extreme ultraviolet) solar fluxes produce the classical photoelectrons (Winningham et al., 1989). Further work indicates that both the classical and the energetic photoelectrons are present in the sunlit polar cap. The focus of our work is to model the electron flux in the polar cap and discriminate between this photoelectron population and the well-known polar-rain population of magnetospheric origin. However, before modeling polar cap data in detail, we must return to the midlatitude data in order to settle some unresolved issues from the preliminary analysis.

3.1 Midlatitude Calculation

In modeling midlatitude electron flux measurements by photoelectron transport calculations, the major issue is the uncertainty in the spectrum of the solar EUV and soft X-ray flux. The solar flux is one of the primary input parameters of such models because its magnitude and spectrum determines the magnitude and variation with energy of the photoelectron source function. Because of the temporal variability of the solar EUV and soft X-ray spectrum, considerable uncertainty might exist in an ab-initio calculation of the electron flux in any individual event. We resolved this issue by turning the question around: by requiring that modeled electron fluxes agree with the satellite observations, we could deduce a possible form for the solar spectrum. This synthetic spectrum could then be used to model the photoelectrons in electron data taken in regions where photoelectrons were not the only constituents, such as the sunlit polar cap. In general, this was a successful approach, in the sense that over most of the wavelength range, the synthetic spectrum did not depart too far from the statistical expectations for the spectrum under the level of solar activity found during the event modeled. In order to obtain detailed agreement with electron flux data between 300 and 600 eV, however, we initially had to use fairly large solar soft X-ray fluxes, especially between 20 and 40 Angstroms (\AA). Improvements and refinements made to the neutral atmosphere model, the photoionization cross sections, the photoabsorption cross sections, and the model parameters, only made the problem worse. Although the solar X-ray spectrum is highly variable, it was not at all clear that our inferred soft X-ray spectrum between 20 and 40 \AA was physically reasonable.

This difficulty prompted a search for processes that might produce "more" high energy electrons. One process we considered was the production of Auger electrons. We found that for O, N₂, and O₂, a K-shell ionization is followed over 99% of the time by an Auger transition that produces another free electron. Further, the energy of that electron is dependent on the neutral species involved but independent of the photon energy. Thus, any photon with enough energy to cause a K-shell ionization will lead to the production of a second electron, the Auger electron, within a narrow energy band at high energy. When we included this process in our model, we found two "bumps" appearing in the photoelectron flux exactly where similar features are seen in the electron flux data. The soft solar X-ray flux needed to fit the data was significantly smaller than that needed when Auger electrons were not included in the calculation.

3.2 Polar Cap Calculation

Having greater confidence in our midlatitude results and the deduced synthetic solar spectrum, we used that solar spectrum in a series of calculations designed to evaluate the role of the photoelectrons in the sunlit polar cap. In these calculations, we considered two different levels of flux for the precipitating polar rain electrons: a typical or moderate level, as characterized in the statistics of the magnitudes of flux observed by DMSP, and a weak level representing the minimal polar rain. For each case, we performed three calculations: a full calculation with both photoelectron and polar rain sources of electrons, a calculation with only photoelectron production (no polar rain), and a calculation with just polar rain (no photoproduction). For both minimum and moderate polar rain, we found that there can easily be conditions where upflowing electrons in the polar cap are dominated by photoelectrons at all altitudes. For downflowing electrons, on the other hand, the importance of the photoelectrons is a very sensitive function of altitude. At 800 km, it appears that the downflowing electrons can be treated purely as a polar rain population. When the polar rain is minimal, the photoelectron population at a representative energy of 100 eV can become important at 600 km while for moderate polar rain, this transition can occur around 300 km. These transition altitudes also depend on the energy being

considered. What does this mean for polar rain studies in the sunlit polar cap? If the data come from a zenith looking instrument onboard a satellite at 800 km, such as DMSP, then the "contamination" by ionospheric photoelectrons will be minimal and the data can be considered "pure" polar rain. On the other hand, data from a satellite such as DE-2, which went as low in altitude as 300 km, may very well include a significant photoelectron population, and the relative contributions of polar rain precipitation and photoelectron production would have to be considered carefully on a case-by-case basis.

To this point, our modeling of ionospheric photoelectron flux data had been done on a case-by-case basis, that is to say, data from different locations had been modeled separately.

We generalized our modeling of low-altitude electron fluxes at moderate energies (20 eV to 1 keV) to be able to calculate the fluxes along a satellite track from the daytime midlatitudes, through the cusp, over the polar cap, and across the nighttime auroral region. In this way, we were able to simulate satellite observations of the electron flux through an entire segment of an orbital pass and compare the theoretical results to the satellite observations. Using this global model, we simulated electron flux data taken on a DE-2 overflight of the northern polar cap. The electron data came from the Low Altitude Plasma Instrument (LAPI) onboard DE-2, from the same pass that was used in our earlier work on energetic photoelectrons in the midlatitudes. For this simulation, the solar flux inferred by modeling electron data at one midlatitude location was used in calculating the photoelectron source function throughout the pass, while the satellite observations of downflowing electron fluxes were used as a boundary condition on the region in which we were solving the electron transport equation. The accuracy of the modeling can then be evaluated by comparing the calculated upflowing electron flux as a function of pitch angle and energy to the flux observed by satellite. At high energies (85-640 eV), we obtained excellent agreement between data and theory at all locations along the satellite track, including the terminator region. At low energies (20-85 eV), we obtained qualitative agreement with the shape of the latitudinal electron flux profile, but we underestimated the magnitude of the electron flux. Because the agreement worsens as photoelectrons make up a smaller fraction of the upflowing flux, we suspected that our treatment of low energy electron backscatter needed improvement. In particular, uncertainties in backscatter cross sections were thought to be a likely source of these errors.

In the electron transport model, the essential mechanism for angular scattering of electrons is the process of electron-neutral elastic collisions. In the model's formulation, the differential cross section for electron-neutral elastic scattering (as a function of energy and pitch angle) is taken to be the total cross section times a normalized phase function, which gives the probability of scattering from one pitch angle to another. The form of the phase function was originally derived from the screened Rutherford formula for the differential cross section (as a function of energy and scattering angle). Using this formula leads to an angular cross section which is generally forward peaked. An examination of experimental cross section data shows that this is a reasonable formulation above 100 eV but the cross sections below 100 eV show a sizeable additional peak in the backward direction. For example, for scattering with N₂ at energies below 50 eV, the Rutherford formula originally used in the model leads to a probability of backward scattering that is over an order of magnitude smaller than that seen in the laboratory.

To examine the sensitivity of the electron transport calculation to the form of the phase function, we made a test calculation using an isotropic scattering approximation below 100 eV. This is still a poor approximation to the measured cross sections but we expected it to give a significantly larger backscatter compared to our original phase function. In this way, we could get some idea whether improving our phase function

would be a useful modification to our model. In the sunlit polar cap, the test calculation showed only small changes from the previous results (as expected, because the low-energy flux here is due to photoproduction and inelastic scattering). Through the terminator, agreement between model and observations improved markedly. In darkness some improvement was seen, but the model electron flux was still significantly below the observations. Our conclusion was that the backscatter is indeed quite sensitive to the form of the phase function and that modifying our formulation of it would be worth the effort.

Accordingly, we modified the electron transport model to use a more precise representation of the angular dependence of the elastic cross section. We chose to follow the approach of Prasad et al. (1985) who used the parameterized elastic cross sections of Porter and Jump (1978). The analytic cross sections consist of two screened Rutherford type terms, and depend on four energy-dependent parameters determined by nonlinear least squares fitting of measured differential cross sections. The form of the cross sections allows an integration over pitch angle to be done analytically and thus, does not increase the computer requirements of the model.

The electron transport model is actually divided into two codes. The first is called MX and it prepares the cross sections into a matrix form for use in solving the transport equation. The second is named B3C and it actually solves the transport equation. The changes in our treatment of the elastic cross sections required modifications to MX but required no changes to B3C.

When comparison with data was made using the new version of the model, we found that at low energies (below 85 eV), we still underestimated the upward electron flux. For example, at 10 eV, the measurements showed an electron flux of 6.0×10^5 ($\text{el cm}^{-2} \text{s}^{-1} \text{sr}^{-1} \text{eV}^{-1}$). The original version of the model gave a flux of 2.0×10^5 while the modified model gave 2.2×10^5 . Clearly, we still had a low energy problem. We then made a series of calculations to investigate the role of several "parameters" in the model, specifically the assumed electron density and the assumed pitch angle distribution of the secondary electrons. We found that if we turned off the energy loss due to Coulomb scattering, the electron flux at 10 eV went to 3.4×10^5 but at 30 eV, there was no effect. Thus, a different assumed electron density would do little to solve our problem. In another calculation, we assumed that the secondary electrons above 10 eV were all forward scattered. This was in contrast to our normal assumption that below 100 eV, the secondaries are produced isotropically. The results were unexpected: the upgoing flux at 10 eV increased to 3.5×10^5 , a 59% increase over our standard calculation. At lower altitudes, we saw an increase of over a factor of four compared to our standard calculation. These results were so surprising, we decided to compare them with results from other versions of the MX and B3C programs. From those comparisons, we discovered that our electron transport model would give dramatically different results below 100 eV when different pitch angle grids were used. The critical difference appeared to be whether the grid was evenly spaced in the cosine of the pitch angle or was non-uniformly spaced. This issue remains unresolved, but it is very possible that when resolved, the problem of underestimating the low energy data will be solved. This is based on the fact that our previous comparisons to data involved calculations on a non-uniform pitch angle grid, whereas when we use the evenly spaced pitch angle grid, we calculate a flux at 10 eV of 5.0×10^5 . This is well within the error bars of the data.

3.3 Future Directions

Our work on electron transport could lead us in a variety of directions. First, the type of analysis that we performed on a segment of one DE-2 orbit could be done systematically on many DE-2 orbits. The purpose would be to test the atmospheric-transport methods of Strickland et al. (1976) under a variety of geophysical conditions. Another topic would involve coupling our transport model with a Monte Carlo simulation of electron scattering in the plasmasphere. The idea would be to develop an electron kinetic model for an entire midlatitude fluxtube. The role of the Monte Carlo simulation would be to simulate adiabatic motion, Coulomb collisions, and wave-particle interactions.

4. PROTON-HYDROGEN ATOM PRECIPITATION

In recent years, the first self-consistent theory for the combined electron-proton-hydrogen atom aurora was developed by D.J. Strickland, B. Basu, J.R. Jasperse, and R.E. Daniell. The theory involves the use of transport theoretic methods to solve a set of three Boltzmann equations for the electron, proton, and hydrogen atom differential fluxes. The protons and hydrogen atoms are coupled to each other by charge-changing collisions (charge exchange and stripping), and the electrons are coupled to the protons and hydrogen atoms because of the secondary electrons that are produced. The new feature of this model over previous work is that the secondary electrons produced by the primary protons and hydrogen atoms are included in the solution of the electron transport equation. The major new and unexpected result from doing this is that the secondary electron flux produced by the proton-hydrogen atom aurora is much softer than that produced by the electron aurora. This is due to the fact that the cross sections for proton and hydrogen impact ionization decrease exponentially with increasing secondary electron energy, whereas the cross sections for electron impact ionization decrease as an inverse power law with increasing secondary energy.

4.1 Comparisons with Observations

Previously, the portions of the model involving just electron transport have been tested against a variety of data. The coupled proton-hydrogen atom segment of the model has had only one type of comparison with data. That is, a calculation of the ionization produced by a specific proton aurora agreed with the ionization that was observed by incoherent scatter radar. Until the work reported here, the coupling between the electrons and the protons and hydrogen atoms was untested.

The greatest difficulty in making such a test was finding a suitable data set. Ideally, you would like a measurement of all three species as a function of altitude, energy, and pitch angle, but such a case was not found. Rather, we took advantage of our access to, and experience with, the measurements made by the Low Altitude Plasma Instrument (LAPI) that was onboard the Dynamics Explorer 2 satellite. This instrument measured electron and ion fluxes as a function of energy and pitch angle. Such data can serve as a limited but useful test of the kinetic model. In particular, it allowed us to test how well the model predicts the upgoing electron flux that results from incident electrons and protons.

As stated above, our primary interest was in the electrons that are produced by incident protons. Our original thought was to look at three cases: the pure proton aurora, the pure electron aurora, and the mixed aurora. But after studying the results of some preliminary calculations, we came to realize that the interesting case would be the pure proton aurora as compared to the pure electron aurora. The mixed aurora is not very

interesting because the soft electron spectrum produced by precipitating protons and hydrogen atoms can easily be masked by the electrons produced by the precipitating electrons. This also meant that in order to study the electrons produced by precipitating protons and hydrogen atoms, we would need a very "pure" proton aurora, that is, precipitating protons and hydrogen atoms with a minimum of coincident precipitating electrons. This need for a very pure proton aurora made finding a suitable case quite difficult. For example, a case used in an E region study that had been identified previously as a pure proton aurora did not come close to being pure enough for studying the electron backscatter in the F region. We realized that we had to be very particular where we looked for proton auroras. Besides looking in the dusk sector equatorward of electron auroras, we also focused on times of the year near equinox. This was done in order to find a case where the ionospheric portions of the fieldline would be in darkness so that there would be no contamination due to photoelectrons produced in the local or conjugate ionosphere.

We found a suitable case from day 289 in 1981 when DE-2 passed through an electron aurora between 19:43 and 19:44 UT and then passed through a fairly pure proton aurora between 19:44 and 19:45 UT. The solar local time was around 21.3 hours and the satellite altitude was around 950 km. At 19:43, the satellite was at an invariant latitude of 72.5 degrees and at 19:45, it was at 66.5 degrees.

This case on day 289, while the "best" we found, was far from ideal. The proton flux was quite modest requiring that we sum over 27 sweeps (27 seconds) to obtain reasonable counting statistics. Further, it was not a pure proton aurora case but rather there was a measurable flux of downgoing electrons. A flux of upgoing electrons that we wished to compare to our model was also measured but this flux was also fairly modest in intensity. So in both the electron and ion data, we were forced to live with the limitations of low counting rates.

Once our data processing was in place, we turned to modeling our case from day 289. As noted above, the measurements were made around 950 km. While we expected that the effects of charged particle-neutral collisions would be small at this high altitude, we wanted, if possible, to calculate them explicitly. But attempts to execute our proton-hydrogen atom code above 600 km ran into numerical problems. After some work, we came to believe that the problem was not an error as such but rather a shortcoming in the design of the algorithm used to solve the coupled proton hydrogen atom transport equations. Fortunately, we had available closed form analytic solutions for this problem that are appropriate at high altitudes. We thus used the analytic solutions from 950 km to 600 km and at 600 km, these solutions were used as the boundary conditions for a full numerical solution at altitudes below 600 km.

For the electron transport part of the model, we decided to limit ourselves to calculations from 600 km down. This was again due to numerical problems. From earlier work we knew that the electron transport code can begin to lose convergence at lower energies as you attempt to solve over larger ranges of altitudes. But based on our previous experiences, we felt it was useful to attempt modeling the electron data as if it were taken at 600 km.

From our first comparisons, we discovered that the model predicts upflowing electrons that are certainly the right order of magnitude. Second, we found that the model results are sensitive to the proton flux above 27 keV. But LAPI only measured ion fluxes up to 27 keV and thus, our results are sensitive to how we extrapolate the incident proton flux to higher energies. Fitting a kappa distribution to the data versus a Maxwellian will lead to almost a factor of 2 increase in the inferred incident proton flux. There is evidence from other satellite measurements that in the plasma sheet, a kappa distribution provides a

much better fit to data than does a Maxwellian (Christon et al., 1988; Christon et al., 1989; Christon et al., 1991). For our case, using a kappa extrapolation gives better agreement with data. A calculation using only the observed incident electron flux clearly underestimates the low energy data (about a factor of three at 50 eV). Above 200 eV, the protons have little effect and the upgoing electron flux results from the incident electrons. If we attempt to match the data by increasing the incident electron flux above 50 eV, we have to use a flux which is well above the observed incident electron flux. Thus, the effects of the protons are clearly important in this case. Given the uncertainties in the data and the need to extrapolate the proton flux, we believe we can claim the model is producing results good to a factor of 2.

To clearly illustrate the contrast between upflowing electrons produced by precipitating protons and hydrogen atoms and those produced by precipitating electrons, we made two calculations. In one case, we used an incident flux of electrons characterized by a 1 keV Maxwellian with a total energy flux of $1 \text{ erg cm}^{-2} \text{ sec}^{-1}$. For the other case, we considered an incident flux of protons characterized by an 8 keV Maxwellian with a total energy flux of $1 \text{ erg cm}^{-2} \text{ sec}^{-1}$. In the proton case, a characteristic energy of 8 keV was chosen because it had been found from earlier calculations that an 8 keV proton Maxwellian produces a volume ionization rate which peaks at about the same altitude as that produced by a 1 keV electron Maxwellian. When we compared the two cases, the resultant energy spectra of the upflowing electrons were dramatically different. Compared to the electron case, the proton case produces a much softer spectrum, a spectrum that for energies above 200 eV is over 4 orders of magnitude smaller than in the electron case. Interestingly, if you examine the total ionization rates for the two cases, you see that they differ only by around 25%.

Using data from the Low Altitude Plasma Instrument (LAPI) that was onboard the DE-2 satellite, we compared the "purest" proton aurora that we found to a pure electron aurora that had about the same incident energy flux. We found clear qualitative agreement with the theoretical prediction. In the proton case, the upflowing electrons above 100 eV were clearly a couple of orders of magnitude smaller than those seen in the electron aurora case.

One step in improving our detailed quantitative modeling of data from day 289 in 1981 was to extend our electron transport upper boundary from 600 km to 900 km. As expected, this led to convergence problems at the lowest energies considered, but we were able to verify that above 30 eV, collisions have very little effect on the upgoing electron flux. Below 30 eV, there was the expected attenuation due to Coulomb collisions with the thermal electrons. Thus, detailed comparisons with data in this lower energy range require both an accurate electron density profile as well as an accurate treatment of the Coulomb collisions.

When we model the low energy upflowing electrons at 900 km, where do they come from? Does it tell us anything about how the model is doing in the E region where most of the energy deposition takes place? To address these questions, a set of calculations was made where we tried different lower boundaries from 98 to 200 km. From these calculations, we found that over 90% of the upflowing electrons below 100 eV come from above 200 km. Thus, modeling the upflowing electrons seen in this particular event on day 289 is a test of how the model does in the F region but says little about its E region performance.

4.2 Future Directions

Our present proton-hydrogen atom model contains no processes that change the pitch angle of the particles. Thus, given an incident downward flux of protons, the model produces no upward flux of protons and hydrogen atoms. On the other hand, an examination of ion measurements made by LAP1 during a proton aurora shows an upward flux of ions at pitch angles near 90 degrees. This suggests that one useful improvement to the model would be to include magnetic mirroring of the protons.

Another obvious need is for more comparisons with observations. In this work, we have examined only a single case of electrons produced by precipitating protons. Further, there have been no comparisons between observations and predicted proton and hydrogen atom fluxes. For any such studies, we suspect that the greatest problem will be finding suitable data. Finally, the optical emissions produced in a three species aurora are another model result that needs to be compared to observations.

5. IONOSPHERIC PLASMA TURBULENCE AND PARTICLE ACCELERATION ASSOCIATED WITH DISCRETE-ARC PRECIPITATION

Auroral hiss is a wave phenomena commonly observed in the acceleration region above the auroral zone, associated with inverted-V electron precipitation. The frequencies of these waves, extending from the lower-hybrid resonance up to the plasma frequency, fall in the VLF range, and their dispersion characteristics have led them to be identified with waves on the whistler resonance-cone plasma dispersion surface. The electric field intensities of these waves are occasionally large, and this turbulence has been observed to be correlated with the energy flux of transversely accelerated ions observed in the topside ionosphere.

A mechanism by which wave-particle interaction of ions with this intense turbulence near the lower-hybrid frequency leads to ion conic formation was suggested by Chang and Coppi: the turbulence is excited by the instability of the ambient plasma combined with the auroral electrons accelerated to drift along the geomagnetic field by the field-aligned potential drop in the supraauroral region. Wave-particle interaction of the ambient ion population with the turbulence near the lower-hybrid frequency leads to ion acceleration nearly perpendicular to the field line, which is followed by the adiabatic folding of velocities as the ions mirror and travel up the field line, to create the conic velocity distribution.

Plasma simulations by us have shown this mechanism to be effective not only for the transverse acceleration of ions, but also for the acceleration of the ambient electrons in the directions parallel to the geomagnetic field. Electron velocity distributions are found to have enhanced fluxes of energetic electrons in both directions with respect to the geomagnetic field, a form which is indeed observed in conjunction with ion conics, where it is called counterstreaming electrons. (We refer here to the counterstreaming electrons of Type "1", in which there is no evidence of electron acceleration by DC parallel electric fields.)

5.1 Two Dimensional Plasma Simulations

In the interest of simplicity, our earlier simulations were one dimensional simulations in which the waves could propagate in only one direction with respect to the ambient magnetic field. A number of interesting phenomena, however, can be realized only in higher dimensions, where a range of propagation angles can be studied simultaneously. For example, both the real frequency and the convective linear growth rates of waves on the whistler resonance-cone dispersion surface are a function of the angle of propagation with respect to the magnetic field. Mode-coupling processes cannot be studied in complete generality in one dimension, because wave vectors there are constrained to be aligned in the same direction. Finally, because electrons and ions interact with different efficiencies to waves of different frequencies, an estimation of the relative effectiveness of electron and ion acceleration requires a simulation in which waves of an appropriate range of frequencies can be excited. To address these questions, a two dimensional simulation model was designed and a series of simulation runs were performed.

In the two-d simulations, strong particle acceleration was observed, both of electrons and of ions. Because of their restricted perpendicular mobility, electron acceleration occurred primarily parallel to the magnetic field. The acceleration caused energetic tail formation on the electron parallel-velocity distribution, both in the direction of the beam and in the opposite direction. The acceleration in the direction opposite to the beam, as well as the initial acceleration in the beam direction, can be attributed to resonant interaction with short-wavelength waves excited by the nonlinear decay of the long-wavelength waves excited linearly by the beam. The ions tend to be accelerated in the direction perpendicular to the magnetic field and lighter ions are accelerated to greater individual energies than heavier ions are. These are both consequences of the resonant nature of the interaction with the waves: the perpendicularly propagating waves have lower frequencies and phase velocities so the ions can more easily interact with them, and the lighter ions have higher thermal velocities and will be more likely to match the phase velocity of a wave. The mass dependence of the velocity diffusion coefficient also favors the acceleration of the lighter ion species. Given the observed wave spectrum, the quasilinear description of particle acceleration appears to be adequate to account for both the electron and ion acceleration observed.

Much of the interesting physics of the simulation is contained in the evolution of the waves, which can be viewed by means of simulation snapshots of electric-field spectral densities with respect to frequency and wavevector. In the classic picture, waves are generated at relatively long wavelengths by the linear instability; once these waves become intense enough, they succumb to a variety of nonlinear mode-coupling processes which attempt to thermalize and isotropize the spectrum. This process can be documented with the snapshots from the simulation. The mode-coupling processes also aid particle acceleration by making the excited waves more accessible in phase velocity to the low-energy ions and electrons. Spectral analysis of the temporal evolution of the potential at one position helps us identify the waves that an in-situ observer would measure. Doing this, we find a broadband spectrum of frequencies, ranging from the lower hybrid resonance frequency up to the plasma frequency. Note that if a one-dimensional simulation of the situation had been performed, only the plasma frequency waves, due to their stronger linear coupling with the auroral electrons, would have been produced. The observations of auroral hiss indicate that the spectrum of the turbulence is in fact broadband like the results of the two dimensional simulations. Thus we see the importance of the generalization to a simulation model with more degrees of freedom. Because ions can resonantly interact only with low-frequency waves, their demonstrated acceleration in the two-d simulations and in space reinforces this conclusion.

5.2 Comparisons to Observations

Another aspect of our study of ion acceleration in the topside ionosphere involves the analysis of observational data and the application of theoretical models to the data in order to test and refine the models. The rocket flight MARIE gave us what is probably the best set of data illustrating the formation of ion conics through the wave-particle interaction of ions with intense VLF turbulence. Ion flux detectors recorded energetic ion fluxes near pitch angles of 90 degrees, indicating that the transverse heating of the ions was occurring in the vicinity of the rocket. Mass spectrometer data showed that the energetic ions were predominantly H⁺. Simultaneously, electric field measurements indicated an intense auroral hiss spectrum, with its low-frequency cutoff at the lower hybrid frequency. Although the intensities of the ion flux and electric field correlated strongly with one another during the relevant portions of the flight, it was still necessary to establish that the waves are responsible for the heating.

To do this, we performed a series of Monte Carlo simulations of the event, using the observed electric fields to heat the ambient ion population to determine if the turbulence can heat the ions to the observed energies. Pitch-angle data gave us some information about the geometry of the event and the extent of the heating region, which was less than 100 km along the geomagnetic field line. Without information about the wave-vector spectrum of the waves, we had to rely on either models of the k-spectrum or simple order-of-magnitude estimates of it, because the wave-particle resonance is a velocity-dependent one. For these calculations, we used the latter, and from the intensity of the electric field spectrum, estimated that the H⁺ heating rate was about 0.8 eV/sec.

From the Monte Carlo calculations, we found that the turbulence heats the H⁺ ions to an average energy of about 7 eV, starting from an initial temperature of 1 eV, with measurable ion flux out to 100 eV. This is smaller than the observed energy; the observed temperature is 22 eV, with ion flux out to 400 eV. With the remaining uncertainties in the model, however, the fact that these predicted energies are comparable to the observed energies is a signal of success. It is to be noted especially that if the waves of the turbulence are being absorbed by the ions as they are being excited in the plasma, the measured level of the electric field will not be a true measure of the strength of the ion heating rate.

5.3 Future Directions

One of the consequences of the inhomogeneity of density and magnetic field in the topside ionosphere is expected to be the processes by which the characteristics of plasma waves generated in one region of space change as the waves propagate to other regions. To examine the role that these processes play in determining the nature of the plasma waves and particle acceleration observed in the auroral zone, a set of plasma simulations could be designed. By launching whistler resonance-cone waves into a density gradient, one could investigate the propagation of the waves into the region where their frequency meets the local lower-hybrid resonance frequency and they are either absorbed directly or converted into shorter wavelength waves which can perhaps be more efficiently absorbed by the ambient plasma populations. In this way, it is expected that the mode conversion process acts as an aid to the production of transverse ion acceleration into the ion conics that are observed in the region.

6. MODELING THE IONOSPHERIC E-REGION

Over the years, many researchers have developed E region models, ourselves included, but a common problem has been a tendency of the models to underestimate the electron density when compared to observational data. While a variety of reasons have been considered, we have found in the literature no definitive resolution to this problem. As recently as 1988, Rasmussen et al. (1988) discussed this problem and concluded that little improvement was possible at that time due to uncertainties in solar fluxes, reaction rates, cross sections, etc. More recently, Buonsanto (1990) compared daytime model results with ionosonde data over a full solar cycle, a variety of Millstone Hill radar data, and a couple of ion composition models. While recognizing the same problems noted by Rasmussen et al. (1988), Buonsanto (1990) had reasonable success between 110 and 180 km if (1) the standard EUV solar fluxes were increased by 25-30% and (2) the neutral densities given by MSIS-86 were decreased.

6.1 Auger Electron Effects

In section 3.1, we described the role of solar soft X-rays and Auger electrons in contributing to the high altitude energetic photoelectron flux. In this section, we describe our study of the effects of solar X-rays and Auger electrons on the Earth's E-region. Using a local steady-state model of the Earth's E-region, we have found that the importance of the Auger electrons depends critically on the intensity of the solar soft X-rays and the solar zenith angle (SZA). At large SZAs during solar maximum, we found the most dramatic effects from the Auger electrons, whereas during solar minimum and at small SZAs, the effects are much reduced. The quantities most affected are those that depend directly and simply on the photoelectron flux, such as airglow volume emission rates and electron secondary production rates. On the other hand, quantities with less sensitivity to the photoelectron flux, such as the electron and ion densities, are less affected. The largest uncertainty in evaluating the role of the Auger electrons comes from our lack of knowledge concerning the intensity of the solar soft X-rays, a region of the solar spectrum that is highly variable and inadequately measured. In an attempt to evaluate the most appropriate solar fluxes to use, we surveyed the available measured solar fluxes and the scaling models derived from them. One constraint on the solar flux might be made by requiring that an E-region model using the flux produce an E-layer density which is in agreement with empirical E-layer models, which are based on observations of E-region densities. With this in mind, we made a series of calculations of the E-region electron density profile using the Hinteregger reference flux SC#21REFW and the associated F10.7 algorithms. We found that the E-region peak density predicted by our theoretical E-region model is consistently less than that predicted by an empirical E-region model. To get agreement in the solar minimum case (F10.7 = 77), a scaling factor of 3.4 was applied to the high energy solar flux ($E < 88$ eV). While not small, this scaling of the flux is reasonably consistent with the findings of other workers. One difficulty in this approach is that the solar flux is not the only input of theoretical E-region models which is known to be subject to large uncertainty or natural variability. In particular, consideration of the role of NO in the model led us to develop an improved characterization of the NO altitude profile.

6.2 Global Modeling

In order to complement our ability to model the F region of the Earth's ionosphere on a global scale, we extended what was an E region daytime model to include the nighttime E region. This involved implementing a nocturnal source of ionization similar to that in our F region model. For the E region, we included the production of N_2^+ and O_2^+

as well as O+, and we included photons at a fourth wavelength (1026). In order to handle the large solar zenith angles around sunset and sunrise, our calculation of neutral column density was completely rewritten. Previously, we had used the secant approximation for angles less than 80° and used Chapman's grazing incidence approximation for angles up to 90°. While the Chapman approximation can be used for angles above 90°, our approach had the problem of causing a discontinuity when we switched from the secant to the Chapman approximation. This was true even when we shifted the cross over point to lower angles. Our new version does line of sight numerical integration at angles above 23.5° and uses the secant approximation below, giving a highly accurate and smoothly-behaving column density. In addition to a nighttime capability, the model can now be run over a grid of longitudes, latitudes, and times.

6.3 Future Directions

As mentioned, in our model we have scaled the solar soft X-ray flux above the values given in published reference spectra. While this has helped bring the modeled FoE in agreement with observations, between the E layer and F2 layer peaks, we still see the tendency to underestimate the observations. Future work should involve a study of the sensitivity of the model to variations in neutral density, electron temperature, recombination rates, and O+(2D) chemistry. The purpose would be (1) to see if you would have any success with the scalings suggested by Buonsanto and (2) to see what fine tuning of the model will reproduce reasonable E regions.

To make further progress on the role of the solar soft X-rays, one could do a detailed analysis of coincident data from the Low Altitude Plasma Instrument on DE-2 and ground based digisondes. In such a study, you would use a measured electron spectrum to infer a solar flux and then use that flux to calculate an E-region electron profile. That profile would, in turn, be compared to a digisonde measured profile.

7. MODELING THE MIDLATITUDE F-REGION

7.1 Model Modifications

Over the life of the contract, we have made a series of modifications to our theoretical O+ F-region model. The first modification was implementing the horizontal wind model (HWM87) of Hedin et al. (1988) into our code. This is an empirical neutral wind model based on wind data obtained from the Atmosphere Explorer E and Dynamics Explorer 2 satellites. With HWM87, we could then include zonal winds in our model, but to take advantage of this, we needed to include the magnetic field declination. From earlier work (Rush et al., 1984), we knew that including the zonal wind and magnetic declination is an essential element in modeling the longitude/UT dependence in the F region ionosphere. At the time of the earlier studies, reliable neutral wind models for use in ionospheric modeling were not available. But with models available such as HWM87 and the Vector Spherical Harmonic model of Killeen et al. (1987), the time was right for studying the importance of the ionospheric effects of the zonal wind and magnetic declination.

Two other inputs to our F-region model are the Te and Ti profiles and they can have a strong impact on a model's ability to agree with measurements. The original model used an empirical Te and Ti model based on Strobel and McElroy (1970). We have now upgraded both the Te and Ti models. For Te, we decided not to use the model as found in the International Reference Ionosphere (IRI) but to implement our own version of the

global empirical Te model of Brace and Theis (1981). This model gives Te at 300 and 400 km as a function of season, dip latitude, and local time. We constructed an entire profile through a combination of linear interpolation and a profile shape function based on Millstone Hill radar data (Strobel and McElroy, 1970). For the ion temperature, we turned to ion temperature measurements made at Millstone Hill for the year 1964 (Evans, 1967). From this data, we constructed a tabulation of Ti at 400 and 600 km as a function of season and local time. The entire profile is again constructed through a mixture of linear interpolation and a profile shape function.

The next changes involved implementing new diffusion and chemistry rates so as to be consistent with existing low and high latitude models. Finally, we improved our daytime source of O⁺ in our F region model. Originally, the source was calculated using a very crude approximation. The solar flux was characterized by a single number and the absorption of photons in the atmosphere was calculated using a single cross section. Further, there was no explicit source due to secondary ionization, but rather it was poorly approximated by not allowing O⁺(2D) to be converted to N₂⁺. The result was that while computationally fast, these approximations severely underestimated O⁺ production at lower altitudes. When calculating the full electron density profile, we could compensate by using at lower altitudes the O⁺ density from our E region model. This meant that in order to get a full O⁺ profile, we had to run both models. On the other hand, especially for global modeling, we wanted to be able to use the F region model's results directly without depending on the E region model. Unfortunately, the complete calculation of the O⁺ source, which we use in our E region model, is too slow for use in the F region model. Thus, we have developed an O⁺ source routine which is sufficiently accurate but fast enough for our purposes. It divides the solar flux and various cross sections into 11 energy bins and includes a calculation of the photoionization of O, a calculation of the dissociative photoionization of O₂, and an estimate of the electron impact ionization of O based on the work of Richards and Torr (1988). This gives a much improved bottomside O⁺ profile and allows the calculation of the total electron density profile by simply adding O⁺ and H⁺ profiles from the F region model with O₂⁺ and NO⁺ from the E region model.

7.2 Theoretical Studies

In this section, I describe two studies: (1) the role of the zonal wind and magnetic declination and (2) a sensitivity study. I begin with the zonal wind study. The importance of including the effects of neutral winds in any solution of the continuity equation is that in the F region the neutral wind moves ionization along geomagnetic field lines. When considering this interaction, it is usually the meridional component of the neutral wind that gets all the attention. This is because the magnetic field is roughly aligned with the meridional wind such that the equatorward meridional wind moves ionization up in altitude, and the poleward meridional wind moves ionization downward. However, this alignment is not exact. Rather, the magnetic field does have a declination and thus, the zonal component of the neutral wind can have a projection along the field. The result is that the zonal wind imparts an upward or downward drift to the ionization depending upon the relative direction between the wind velocity and the declination of the geomagnetic field. The interaction between the zonal wind and the geomagnetic field gives rise to very different diurnal variations of the O⁺ density profile at eastward and westward declinations. It is expected that the clearest signature of this effect can be found by looking at the longitude dependence of the diurnal behavior of the O⁺ profile. While this effect was studied by Rush et al. (1984), they used a fairly simple neutral wind as well as a neutral atmosphere with no longitudinal dependence. By using the horizontal wind model (HWM87) of Hedin et al. (1988), along with the MSIS86 neutral atmosphere, we can do a

more through study of diurnal variations at different longitudes and hence, a more complete assessment of the importance of the zonal wind and magnetic declination.

For our first sets of calculations, we used a tilted dipole magnetic field model to specify the magnetic inclination and declination. We made some initial calculations at two locations that had different longitudes (12 east and 210 east) but had the same geographic (40 north) and geomagnetic (40.8 north) latitudes. In this way, we could examine the differences that arise between locations with the same solar forcing and inclinations but different longitudes. We found that there were differences in the O+ densities at these two locations. For example, an examination of the diurnal variation of the total ion content (TIC) found that at 1000 local time (LT) the TIC at 210 east is 50 percent higher than the 1000 LT TIC at 12 east. At night, this relationship was seen to reverse and the 2200 LT TIC at 12 east was three times larger than that at 210 east.

Our next step was to expand our calculations to a more global scale. The first global calculations were for the northern hemisphere at two geomagnetic longitudes (90.98 (E) and 269° (E)) and over a range of geomagnetic latitudes (70(N) to 26(N)). The tilted dipole model for the Earth's magnetic field gave declinations at these two longitudes opposite in sign and ranging in magnitude from 37.4 to 13 degrees. At a given geomagnetic latitude, each longitude had the same inclination and geographic latitude.

The calculations done for just two locations had given us our first examples of longitudinal differences, but as we began the global calculations, we came to appreciate that a longitudinal dependence does not simply reflect differences in the magnetic declination. Rather, within the context of the model at a fixed latitude, the longitudinal differences in the diurnal behavior are due to differences in declination, longitudinal dependencies in HWM87, and longitudinal dependencies in the MSIS86 neutral atmosphere model. To separate these three effects, we made three sets of calculations. The first set consisted of full calculations of the diurnal behavior of the O+ density along the two magnetic longitudes given above. The second set were the same calculations except the declinations were set to zero, which effectively turned off the zonal wind. In the third set, we repeated the calculations except both components of the neutral wind were set to zero.

From the first set, we find variations with longitude at all latitudes similar to what we saw at one latitude. The general features are the same from latitude to latitude though the quantitative details do vary markedly. These differences in detail reflect the latitudinal dependence of the declination and inclination as well as the latitudinal dependencies contained in the HWM87 wind model and the MSIS86 neutral atmosphere model.

When we focus on a given latitude and compare the results from the different sets, the different longitudinal effects become apparent. Comparison of set 1 and set 2 illustrates the role of the zonal wind and magnetic field declination. We find that at 30 degrees latitude from 0800 to 1300, most of the variation with longitude arises from differences in declination and any longitudinal dependencies in the HWM87 zonal winds. From 1300 to 0600, the variation with longitude is partially effected by zonal winds and declination but a large percentage of the variation is due to longitudinal variations of the meridional wind and/or longitudinal variations in the MSIS86 neutral atmosphere.

Comparisons of set 1 and set 3 show that the neutral atmosphere plays no role in the longitudinal variations at night and for this case, at 30 degrees, a small role around noon. Set 3, with no neutral winds, does illustrate the general point that the neutral winds do make a dramatic difference in the calculated O+ densities. A direct examination of the neutral winds at the two longitudes shows that they are consistent with the variations with longitude seen in the O+ densities. Again, these features are seen at all latitudes to differing

degrees. From these initial results, we see that the diurnal variation of the F2 region is strongly effected by the zonal wind and magnetic declination, as well as the longitudinal and latitudinal variations in the meridional wind.

We expanded on this initial work by including a more thorough parameter study. That is, in the initial calculations, we had considered just one set of geophysical conditions. Now, we made calculations for three seasons (March equinox, June solstice, and December solstice) and three levels of magnetic activity ($A_p = 5, 11, 32$). We also did sets of five calculations for each combination of geophysical conditions. In the first calculation of a set, we calculated the diurnal behavior of the O+ density with the longitude dependence in both HWM87 and MSIS86 turned off and the zonal wind set to zero. In the next, we had the longitude dependence in MSIS86 turned on. The third calculation had the longitude dependence in MSIS86 turned on and included a longitudinally independent zonal wind. The fourth had the zonal wind set back to zero but included a longitude dependent meridional wind from HWM87 along with the longitudinally dependent MSIS86. Finally, the fifth calculation had all the longitude dependencies turned on and included the zonal wind. In total, 90 simulations of the northern midlatitudes were conducted.

What we found was consistent with our earlier results. All three factors described above played a role. In general, the critical sources of longitude differences were zonal/declination differences and the longitude dependence of the meridional wind given by HWM87. The observed differences in the daytime morning were dominated by zonal/declination effects, while the nighttime differences were driven by a mix of zonal/declination effects and longitude dependent meridional winds. While the details varied, the above description was true at all latitudes, seasons, and magnetic activities that we considered. The effects tended to be larger as you approached the equator. They were also larger for more active magnetic conditions. The largest effects were in the summer and the smallest in winter. In all cases, in the daytime morning, the 91° (E) longitude calculation produced smaller densities than the 269° (E) calculation, and at night the reverse was true.

In our second study, we made a series of calculations where we individually varied many of the inputs of the model. Two of these calculations involved variation of microscopic parameters: the O-O+ collision cross section and the fraction of O+(2D) that converts to N₂+. The remaining calculations involved variations of the different geophysical inputs: the electron temperature, the atomic oxygen density, the neutral molecular densities, the solar flux, and the neutral wind. All of these parameters effect the F2 peak density but only the molecular densities and the neutral wind have any significant effect on the F2 peak altitude.

There has been some debate in the recent literature as to whether the accepted value for the O-O+ collision cross section should be increased. Increasing the cross section by the suggested factor of 1.7 leads to just a 5% change in the F2 peak density. Going from one extreme of having all the O+(2D) convert to N₂+ to having none of it convert produces a 35% increase in the F2 peak density. Turning to the electron temperature, we find that a 30% scaling leads to just a 5% effect on the peak density. For both the atomic oxygen and the entire solar flux, the modeled F2 peak density shows a basically linear dependence.

As mentioned, the molecular neutral densities effect both the F2 peak density and altitude. A 30% variation in N₂ and O₂ leads to a 15 to 20% variation in the peak density and a 10 km variation in the peak altitude. But of greatest interest is the neutral wind because it not only effects both the peak height and density but is probably the geophysical input that is most variable and least known. For example, a 50% reduction of the neutral wind from the Hedin et al. (1988) wind model (HWM87) can lead to a 12% increase in the peak density and a 15 km increase in the peak height. Further, if we use the vector

spherical harmonic (VSH) wind model of Killeen et al. (1987) rather than HWM87, we get a peak density 22% larger than that from HWM87 and a peak altitude 25 km higher. An examination of the daytime meridional winds from these two models shows significant differences which lead to the differences seen in the F2 peak parameters. In principle, these two models are describing the neutral wind field for the same geophysical conditions. These differences in results illustrate two points: (1) an ionospheric model is very sensitive to uncertainties in the neutral wind and (2) present wind models can predict significantly different winds under identical geophysical conditions. Our conclusion is that, of all the inputs to our ionospheric model, the neutral wind is the most likely candidate as a major source of error.

7.3 Comparisons with Observations

As part of our development of a daytime E and F region ionospheric model, we analyzed a series of experiments involving observations by the Millstone Hill Radar facility coincident with daytime overflights by a DMSS satellite. Observations were made from February to October 1989 involving the F9 satellite (0930 local time) and the F8 satellite (1800 local time). The early experiments consisted of approximately four hours of radar elevation scans. This produced a time history of the electron density profile (EDP) before, during, and after a satellite overflight. In later experiments, by considering only very close overflights, the Millstone zenith antenna was used in the high resolution OASIS (Optimal Analysis of Signals from Incoherent Scatter) mode and the steerable antenna was used to obtain vector drift measurements.

We performed an analysis on ten experiments using our F and E region models and our generalized-inverse least squares (GILS) algorithm. The GILS algorithm was developed in earlier studies on the use of daytime airglow for remotely sensing the EDP. In this analysis, we ran our ionospheric models in both their ab initio and one constraint mode. In the one constraint mode, we use the measured ion density at the satellite altitude as an indirect constraint on the geophysical input parameters of our models. By using the GILS algorithm to find the most likely set of input parameters for which our model matches the observational constraint, we calculated the most likely electron density profile (EDP). This one constraint result can be compared with the ab initio result and the radar profile, as well as the EDPs predicted by the International Reference Ionosphere (IRI) and the Ionospheric Conductivity and Electron Density (ICED) model. In general, we found that our models in either of their modes perform better than IRI and are comparable to ICED.

While we had made a few comparisons with Millstone radar data and DMSP in-situ data, most of our time had been spent on modifying our model and examining the theoretical results that it produced. Thus, we saw a real need to focus on whether our results were realistic and if our results agreed with other models. Our approach was to see what "tuning" of our midlatitude F region model was necessary in order to satisfy two criteria: 1) The midlatitude model at its low latitude boundary should agree with a low latitude model at its high latitude boundary and 2) The model should produce realistic densities as compared to monthly mean data or empirical models of monthly means. Our interest was not in attempting to model individual days but rather to see if using "typical" or average inputs in the model would produce a "typical" or average ionosphere.

Our first attempt to deal with both of these issues was a calculation of the diurnal behavior of the F2 peak at solar maximum (F10.7 = 180) in March for Rome, Italy. Initially, we had differences between our midlatitude model and a low latitude model. These differences were found to be caused by various small "bugs" in the low latitude code. When they were corrected, the two models agreed to within a few percent.

Unfortunately, while we achieved agreement between models, agreement with ionosonde data was problematical. While data from March 13-18 gave midday F2 peak densities of $2.1\text{-}2.3 \times 10^6 \text{ cm}^{-3}$, our calculations initially ran around $1.2 \times 10^6 \text{ cm}^{-3}$. By making adjustments in the neutral winds and the O-O+ diffusion coefficient, we were able to increase our midday densities up to $1.5 \times 10^6 \text{ cm}^{-3}$. But obviously, the model still underestimated the data. We were also aware that other modelers had similar problems modeling for solar maximum conditions. With these problems in mind, we decided for the time being to focus on solar minimum conditions.

For the solar minimum case, we focused on comparisons between model calculations and monthly averaged F2 peak density measurements made at Wallops Island, Virginia in March, June, September, and December 1986. Our initial calculations produced daytime densities that were in qualitative agreement with the data, but for three of the months (March, September, and December), our nighttime densities were much lower than what was measured. It was only in our June calculation that reasonable nighttime densities were obtained. The largest differences were found in the December case with calculated O+ densities at night of around 102 cm^{-3} compared with measured densities of around 105 cm^{-3} .

Another problem with the December case was a numerical instability at the higher altitudes (600 - 700 km) that began a bit before midnight and grew until photoionization at sunrise began to build up the O+ densities. At first, this seemed to happen only when using the Brace and Thies electron temperature model, but subsequent calculations showed that the instability could also appear when using our older temperature model. We came to believe that the problem was related to the extremely small densities that we were producing at solar minimum nighttime. A check of earlier calculations uncovered other cases where smaller instabilities could be seen in the calculations. These cases also involved small nighttime densities.

In examining the December case, we noted that one reason for the small densities at night was that the meridional wind did not turn equatorward until well after sunset. Using the other available wind model, the VSH model of Killeen et al. (1987), gave different results in detail from those gotten using HWM87 but still did not maintain the nighttime densities. While in individual cases, you could argue that the actual neutral wind can be quite different from the neutral wind models we still had to deal with those cases where the model winds were reasonable. To help maintain the nighttime density, we decided to add a nocturnal source of ionization to the model. We used an approach following Knudsen et al. (1977) of simulating the ionization due to scattered EUV photons. We assume that the scattered EUV photons consist of three lines at 834, 584, and 304\AA . We then calculate the photoionization rates as if these three lines are incident at the top of the ionosphere with zero zenith angle with some assumed intensity. Using intensities based on Knudsen et al. (1977) and Chakrabarti et al. (1984), we found that the nocturnal source helps to keep the nighttime densities from going extremely low but has little effect much above a density of a few times 10^3 cm^{-3} .

An examination of the literature showed that maintaining the winter nighttime ionosphere has been a problem for modelers for a number of years. While there has been much debate as to what is the necessary physics to explain the observations, it seemed to us that recent modeling indicated that including hydrogen ions and the coupling between the ionosphere and the plasmasphere will be necessary for any successful modeling of the winter nighttime. Our model did not have this capability; thus we decided to put in an ad hoc source to maintain our nighttime densities. From our initial experiments with this ad hoc source, we found that when the nighttime densities are maintained, the numerical instability problems do not appear.

We next turned to solar maximum conditions by modeling digisonde data taken at Wallops Island in February of 1989. For the month of February, we performed a day-by-day simulation of the entire month. In comparing our results with the Wallops Island data, we examined just the F2 peak density and height. When we compared our average model results to the average daytime behavior of the F2 peak density, we found that the model did a fair job in that it was pretty much within a standard deviation of the observed mean. But on the other hand, the daytime portion of the calculated diurnal shape of the F2 peak density was consistently different from what was observed. The observations consistently had the daytime maximum at around 10:30 whereas the model had the maximum around 14:30. This was true on a daily basis as well as with the monthly average. A quantitative comparison of the averages showed that at 10:30, the model was 20% low, at noon it was 11% low, and at 14:30 it was within 1% of the data. We should note that we did not see the factors of two differences that have been seen in other comparisons.

When we compared the modeled and measured F2 peak heights, similar results were seen. That is, the average model results were within a standard deviation of the monthly averaged data. But a closer examination of the entire month showed that from 10:30 to 16:30, the model was consistently different from the data, predicting an F2 peak height 10 to 20 km smaller than observed.

The next series of solar maximum calculations involved seven stations and four seasons. The stations were Bermuda, Wallops Island, and Millstone Hill in the American longitude sector; Slough, Moscow, and Klammingrad from the European sector; and Xinxiang from the Asian sector. These were designed as monthly mean calculations by using the monthly averaged F10.7 and Ap. The fifteenth of each month was used in all cases and the months chosen were 12/90, 3/90, 6/90 and 10/89, with the exception of Moscow, where the months modeled were 1/90, 5/90, 7/89 and 11/90.

Unfortunately, data became available only for Millstone Hill, Wallops Island, and Bermuda. At Millstone, comparisons have been made for October, 1989; March, 1990; June, 1990; and December, 1990. For the December case, we found that the modeled fof2 at nighttime falls below the scatter in the data at 1 to 2 Mhz below an average of about 5 Mhz. From sunrise until 1000 hours, the model and data increase together, but from 1000 to around 1200, the model runs beneath the monthly scatter again at about 1 to 2 Mhz below daytime maximums between 12 and 14 Mhz. In the afternoon, the model falls in the lower part of the monthly scatter but moving into evening, it falls off a bit faster than the data. Turning to the March case, little can be said other than that the model falls well within the enormous monthly scatter of the data. The October case is similar to December except that the monthly scatter is large enough that the model remains within it. Finally, in June the observations show a very flat diurnal curve in marked contrast to the diurnal behavior seen at other seasons. The model reflects this change in diurnal shape but at all times clearly falls at the high extremes of the monthly scatter and thus, consistently higher than the monthly mean. The difference is in the 1 to 2 Mhz range when using the older O+/O diffusion rate but can be as large as 3.5 Mhz when using the Burnside factor in the diffusion rate.

The comparisons between the modeled and observed hmf2 give a similar mixture of results. In all four cases, the model falls within the monthly scatter of the data. For December, the agreement with the mean is not bad in the daytime but at night, the model runs about 50 km higher than the data. In June we see the opposite, the model is around 50 km higher from 0700 to midnight and gives fair agreement for the rest of the day. March is not bad over the entire day but again the scatter is large. In October, there is a fair

scatter but the model does trend somewhat higher than the mean, similar again to the December case.

For the other locations (Wallops and Bermuda) similar comments can be made. In general, we do best in the winter and have our biggest problems in the summer.

For several of the stations, we were surprised by the results from around June solstice (May - July). For example, the calculation done for Moscow in May showed a diurnal pattern for fof2 that was the opposite of the "textbook" pattern. It peaked just after 2000 hours local time at around 13 Mhz, stayed flat until 0200 hours, began to decrease to a minimum of 9 Mhz just after 1000 hours, stayed flat, and finally around 1800 hours, began to increase towards its maximum. hmf2 showed a large change going from 300 km around noon to over 480 km at around 2200 hours. Similar behavior was seen in July but not in January or November. These results are in disagreement with the predictions of the International Reference Ionosphere (IRI) and the Field-Line Interhemispheric Plasma (FLIP) model. Our initial suspicion that this result was due directly to the neutral wind turned out to be correct. Calculations at Bermuda as well as calculations for Moscow showed that setting the wind to zero significantly modifies both the fof2 and hmf2 giving diurnal curves that are more "normal". An examination of the neutral wind being used from HWM87 showed that a strong meridional wind that hardly ever turns poleward was responsible for our surprising results. The wind used in the FLIP model for Moscow was deduced from the hmf2s predicted by the IRI. This wind was seen to be radically different from that of HWM87 and accounts for the differences between our results and FLIP's. The question as to what is actually going on at Moscow is unanswered since we had no Moscow data to examine. But our Bermuda results, while high compared to the data, did show a diurnal shape that compared well with data. A brief examination of the day-to-day Bermuda data showed that there can be days where the nighttime densities can be a factor of 2 larger than in the daytime.

7.4 Future Directions

Present midlatitude ionospheric models have been successful at reproducing ionospheric climate (Sojka, 1989), but developing models that can reproduce an actual ionosphere for any given instant will require much more extensive comparisons between models and observations. Today, we are in a position to make progress in modeling and testing the midlatitude models on a global scale. The two primary reasons that this is true are as follows. One, computer power has reached the point where a midlatitude model can be run globally for many cases without using an inordinate amount of computer resources. Two, as automatic processing of digisonde data has become available it is becoming feasible to assemble global data sets of fof2 and hmf2. While global data sets of fof2 have been available for years, the labor intensive processing required to make true height analysis made it prohibitive to assemble such data sets of hmf2. Having global datasets in both quantities will serve as an excellent test of how well any model can reproduce an actual midlatitude ionosphere.

8. MODELING THE HIGH-LATITUDE F-REGION

In the high latitude F-region, we were interested in developing a model to study the production and evolution of polar cap patches and auroral blobs. With that in mind, we began updating an existing high latitude model.

8.1 Model Modifications

The first modifications involved changes that we previously had applied to our midlatitude model. They included updated diffusion rates, updated chemistry rates, an improved photoionization source, a nighttime source of ionization, and a new wind model (HWM87). Besides updating various microscopic parameters along with several of the inputs, we also completely rewrote the outer layers of the model. Our purpose was to develop a comprehensive and flexible time-dependent model that would allow us to assess the roles of various processes in creating large-scale structures within the high latitude F-region. The present model can use any of three high latitude convection models (Heelis et al. 1982; Hairston and Heelis, 1990; and Heppner and Maynard, 1987). It operates in what we call a station mode where one selects a particular ground location and the times at which you want to calculate altitude profiles of the O⁺ density. The profiles are calculated by following flux tubes whose trajectories pass over the station at the specified times. In this way, you can simulate an ionosphere as it would be observed by a ground-based instrument such as a digisonde. In a first attempt to study time varying convection patterns, the model can use up to 16 different convection patterns during a single simulation.

8.2 Theoretical Studies

Our first study using our high latitude model consisted of calculating the F2 parameters at Sondrestrom and Qanaq for February 19, 1990 from 8 UT to just after 17 UT. This period was dictated by the availability of IMF, DMSP, and digisonde data. During this period, we defined nine different convection patterns based on drift measurements made by the F8 DMSP satellite. Our first calculation was for Sondrestrom and used just co-rotation without any other convection. This was to establish a baseline with which to assess the effects of including a convection pattern in later calculations. What we saw was that local production at Sondrestrom produced ample ionization as compared to what was observed but was very smooth compared to the highly variable digisonde data. We next made a calculation using a single convection pattern, one of the nine from the period of interest, and found a little more temporal structure as compared to the co-rotation results but still a much smoother result as compared to the digisonde data. Using all nine convection patterns in our simulation gave slightly different results in detail but qualitatively, those results were the same as the one pattern simulation.

After making a similar set of calculations for Qanaq and obtaining similar results, we made a series of calculations designed to examine the sensitivity of our results to initial conditions, particle precipitation, and neutral wind. To test sensitivity to initial conditions, we repeated the nine convection pattern calculation but followed a flux tube's trajectory for 12 hours before it reached Sondrestrom rather than the six hours used in the original calculation. This had the effect of producing much more dramatic variation in the temporal behavior in fof2 at Sondrestrom. On the other hand, calculations including no particle precipitation showed very little structure in either the 6 or the 12 hour trajectory cases. Turning off the neutral wind likewise had an effect of smoothing out some of the structure. So what we are seeing is that in this case, the model can produce some structure but its existence is sensitive to a variety of parameters within the model. But in all cases, the structure produced is smoother than what is observed.

A final set of calculations was made that included a localized "vortex" potential structure added to a global pattern at a fixed location in magnetic coordinates. The effect in this region of more intense electric fields was to cause an increase in the Γ effective used in

calculating the O⁺ loss rates. This in turn leads to a depletion in the F2 peak density even when the vortex only existed for 10 minutes.

8.3 Future Directions

To make further progress, our present model would need two types of improvements: (1) a more flexible and sophisticated handling of time varying convection and particle precipitation and (2) a capability to do global modeling. When these capabilities are available, then an effective study can be made of various scenarios on how to make F region structure.

9. Summary

In this study on ionospheric transport, we have examined a variety of issues using both kinetic and fluid approaches. In our study of electron flow between the ionosphere and magnetosphere, we have focused on two areas: a kinetic model for the diffuse aurora and the role of energetic photoelectrons within the polar cap. The kinetic model of the electron flux in the diffuse auroral region emphasizes the consequences of pitch-angle scattering, convection, and ionospheric coupling on the electron population. We found that when pitch angle scattering is not strong, a model with precipitation alone cannot explain the equatorward edge of the diffuse aurora. In our one dimensional model, a drift-boundary limitation of flux must be imposed in order to produce a realistic-looking equatorward edge. In our two dimensional model, a realistic edge can be produced as the results of energy-dependent gradient/curvature drifts of the electrons.

In our work on the sunlit polar cap, we have shown experimentally and theoretically that the energetic electron population has an ionospheric source (photoelectrons) and a magnetospheric source (polar rain). We find that at low energies, our theory is in quantitative agreement with observations except for about a factor of 2 in the low energy backscatter. At high energies, there is excellent quantitative agreement between theory and experiment.

Our study of ion flows between the ionosphere and magnetosphere also focused on two areas: a test of the first self-consistent theory for the combined electron-proton-hydrogen atom aurora and simulations of ion acceleration. The test of our coupled three species auroral model consisted of calculating the upgoing electrons that result from downgoing protons incident at the top of the ionosphere. Measurements from the Low Altitude Plasma Instrument on board the Dynamics Explorer 2 satellite provided both the needed boundary conditions and the resultant upgoing electron fluxes with which the model results were compared. We found that within the limitations of the data that the agreement between model and data was good.

Two types of simulations were performed to study ion acceleration. First, two dimensional plasma simulations were used to study the generation of broadband turbulence and the resultant particle acceleration. From these simulations, it was found that a broadband spectrum of frequencies, spanning the observed range of auroral hiss, could be excited and that ion acceleration would result. Second, mesoscale (Monte Carlo) simulations were used to analyze ion conic measurements from the rocket flight MARIE. What we found was that the observed turbulence could heat protons from 1 eV to 7 eV. While an underestimation of what was observed, this amount of heating is the right order of magnitude.

Fluid models of the E and F region have been developed to complement our kinetic models. The region model can be used globally and has been adjusted to produce a more realistic FoE. The F region model has both a midlatitude and a high latitude version. The midlatitude version has been tested against a variety of measurements and has been found to reproduce much of the ionospheric climatology. On the other hand, its ability to specify the F region at a given time and place is clearly limited by present uncertainties associated with the inputs to the model. The high latitude F region model is at a much less advanced stage of development and there is much to learn about how it behaves under various conditions.

Over the period of the contract, nine papers were written and twenty-one presentations were given at various national and international scientific meetings. The nine papers are listed below.

Chang, T., G.B. Crew, J.M. Retterer, and J.R. Jasperse, Ionic Conics and Counterstreaming Electrons Generated by Lower Hybrid Waves in the Earth's Magnetosphere, *IEE Trans. Plasma Sci.*, 17, 186, 1989.

Daniell, R.E. Jr., D.T. Decker, D.N. Anderson, J.R. Jasperse, J.J. Sojka, and R.W. Schunk, A Global Ionospheric Conductivity and Electron Density (ICED) Model, in Proceedings of the 6th International Ionospheric Effects Symposium, p. 351, 1990.

Decker, D.T., and J.D. Winningham, Energetic Atmospheric Photoelectrons Due to Solar X-Rays and Auger Production, in Physics of Space Plasmas, ed. by T. Chang, G.B. Crew, and J.R. Jasperse, SPI Conference Proceedings and Reprint Series, Vol. 8, p. 199, 1989.

Decker, D.T., J.R. Jasperse, and J.D. Winningham, Energetic Photoelectrons and the Polar Rain, in Physics of Space Plasmas, ed. by T. Chang, G.B. Crew, and J.R. Jasperse, SPI Conference Proceedings and Reprint Series, Vol. 9, p. 15, 1990.

Reinisch, B.W., D. Anderson, R.R. Gamache, X. Huang, C.F. Chen, and D.T. Decker, Validating Ionospheric Models with Measured Electron Density Profiles, submitted to Proceedings of COSPAR 1992, Washington, DC.

Retterer, J.M., D.T. Decker, and J.R. Jasperse, A Kinetic Model for the Diffuse Aurora, in Physics of Space Plasmas, ed. by T. Chang, B. Coppi, and J.R. Jasperse, SPI Conference Proceedings and Reprint Series, Vol. 7, p. 167, 1988.

Retterer, J.M., and T. Chang, Plasma Simulations of Intense VLF Turbulence and Particle Acceleration in the Supraauroral Region, ed. by T. Chang, G.B. Crew, and J.R. Jasperse, SPI Conference Proceedings and Reprint Series, Vol. 8, p. 309, 1989.

Winningham, J.D., D.T. Decker, J.U. Kozyra, J.R. Jasperse, and A.W. Nagy, Energetic (> 60 eV) Atmospheric Photoelectrons, *J. Geophys. Res.*, 94, 15335, 1989.

Yasseen, F., J.M. Retterer, T. Chang, and J.D. Winningham, Monte Carlo Modeling of Photoelectron Distributions with Anomalous Heat Flux. *Geophys. Res. Lett.*, 16, 1023, 1989.

There are five major computer models that have been developed under this contract. In all five cases, they are modified or extended versions of earlier Air Force developed models. They are:

- (1) Photoelectron transport model
- (2) Proton-hydrogen atom transport model
- (3) E region model
- (4) Middle latitude F region model
- (5) High latitude F region model

REFERENCES

- Brace, L.H., and R.F. Theis, Global empirical models of ionospheric electron temperature in the upper F-region and plasmasphere based on in-situ measurements from Atmosphere Explorer-C, ISIS-1 and ISIS-2 satellites, *J. Atms. Terr. Phys.*, *43*, 1317, 1981.
- Buonsanto, M.J., A study of the daytime E-F₁ region ionosphere at mid-latitudes, *J. Geophys. Res.*, *95*, 7735, 1990.
- Chakrabarti, S., R. Kimble, and S. Bowyer, Spectroscopy of the EUV (350 - 1400Å) nightglow, *J. Geophys. Res.*, *89*, 5660, 1984.
- Christon, S.P., D.G. Mitchell, D.J. Williams, L.A. Frank, C.Y. Huang, and T.E. Eastman, Energy spectra of plasma sheet ions and electrons from ~ 50 eV/e to ~ 1 MeV during plasma sheet temperature transitions, *J. Geophys. Res.*, *93*, 2562, 1988.
- Christon, S.P., D.J. Williams, D.G. Mitchell, L.A. Frank, and C.Y. Huang, Spectral characteristics of plasma sheet ion and electron populations during undisturbed geomagnetic conditions, *J. Geophys. Res.*, *94*, 13409, 1989.
- Christon, S.P., D.J. Williams, D.G. Mitchell, C.Y. Huang, and L.A. Frank, Spectral characteristics of plasma sheet ion and electron populations during disturbed geomagnetic conditions, *J. Geophys. Res.*, *96*, 1, 1991.
- Evans, J.V., Midlatitude F-region densities and temperatures at sunspot minimum, *Planet. Space Sci.*, *15*, 1387, 1967.
- Fontaine, D., and M. Blanc, A theoretical approach to the morphology and the dynamics of diffuse auroral zones, *J. Geophys. Res.*, *88*, 7171 (1983)
- Hairston, M.R., and R.A. Heelis, Model of the high-latitude ionospheric convection pattern during southward interplanetary magnetic field using DE-2 data, *J. Geophys. Res.*, *95*, 2333, 1990.
- Hedin, A.E., N.W. Spencer, and T.L. Killeen, Empirical global model of upper thermosphere winds based on Atmosphere and Dynamics Explorer satellite data, *J. Geophys. Res.*, *93*, 9959, 1988.
- Heelis, R.A., J.K. Lowell, and R.W. Spiro, A model of the high-latitude ionospheric convection pattern, *J. Geophys. Res.*, *87*, 6339, 1982.
- Heppner, J.P., and N.C. Maynard, Empirical high-latitude electric field models, *J. Geophys. Res.*, *92*, 4467, 1987.
- Kennel, C.F., Consequences of a magnetospheric plasma, *Rev. Geophys. Space Phys.* *7*, 379, 1969.
- Killeen, T.L., R.G. Roble, and N.W. Spencer, A computer model of global thermospheric winds and temperatures, *Adv. Space Res.*, *7*, 10207, 1987.

- Knudsen, W.C., P.M. Banks, J.D. Winningham, and D.M. Klumpar, Numerical model of the convecting F2 ionosphere at high latitudes, *J. Geophys. Res.*, *82*, 4784, 1977.
- Porter, H.S., and F.W. Jump, Analytic total and angular elastic electron impact cross sections for planetary atmospheres, Tech. Rep. CSC/TM-78/6017, Computer Sciences Corp., Greenbelt, 1978.
- Prasad, S.S., D.J. Strickland, and Y.T. Chiu, Precipitating electron interaction with the atmosphere, 2, the dayside cusp region, *J. Geophys. Res.*, *90*, 11025, 1985.
- Rasmussen, C.E., R.W. Schunk, and V.B. Wickwar, A photochemical equilibrium model for ionospheric conductivity, *J. Geophys. Res.*, *93*, 9831, 1988.
- Richards, P.G., and D.G. Torr, Ratios of photoelectron to EUV ionization rates for aeronomic studies, *J. Geophys. Res.*, *93*, 4060, 1988.
- Rush, C.M., M. PoKempner, D.N. Anderson, J. Perry, F.G. Stewart, and R. Reasoner, Maps of FoF2 derived from observations and theoretical data, *Radio Sci.*, *19*, 1083, 1984.
- Sharber, J.R., T. Chang, B. Coppi, and J.R. Jasperse, eds., The continuous (diffuse) aurora and auroral-E ionization, in *Physics of Space Plasmas*, p. 115, (Scientific Publishers, Inc., Cambridge MA 1981).
- Sojka, J.J., Global scale, physical models of the F region ionosphere, *Rev. Geophys.*, *27*, 371, 1989.
- Strickland, D.J., D.L. Book, T.P. Coffey, and J.A. Fedder, Transport equations technique for the deposition of auroral electrons, *J. Geophys. Res.*, *81*, 2755, 1976.
- Strobel, D.F., and M.B. McElroy, The F2-layer at middle latitudes, *Planet. Space Sci.*, *18*, 1181, 1970.
- Winningham, J.D., D.T. Decker, J.U. Kozyra, J.R. Jasperse, and A.W. Nagy, Energetic (> 60 eV) atmospheric photoelectrons, *J. Geophys. Res.*, *94*, 15335, 1989.